

RESEARCH

Open Access



Glycolysis and signal transduction participate in *Lycium barbarum* in response to NaCl stress through protein phosphorylation

Wangli Liang^{1†}, Zheng Zhang^{1†}, Ning Yao¹, Bo Wang², Wenjing Yu¹, Qiang Zhu^{1,3}, Shujuan Yang¹, Jijuan Zeng^{1,3}, Lingxia Wang^{1*} and Wenyu Liang^{1,3*}

Abstract

Background *Lycium barbarum* L. possesses great salt tolerance and medicinal values, studying its salt tolerance contribute to variety improvement, as well as the increase in yield and quality.

Results The study integrated the tandem mass tags (TMT) phosphoproteomics and physiological indexes of *L. barbarum* exposed to different concentrations of NaCl, with the aim of characterizing salt adaptation characteristics of *L. barbarum*. The findings indicated that a total of 2189 differentially phosphorylated peptides were identified, functional analysis revealed their involvement in glycolysis, plant hormone signal transduction, mitogen-activated protein kinase (MAPK) signal transduction and other pathways, and that the enzyme activities and substances related to glycolysis and signal transduction underwent significant changes under salt stress.

Conclusion Salt stress enhanced the glycolysis pathway through protein phosphorylation, and the changes in related enzymes activity accelerated the conversion of intermediate metabolites and energy supply. Salt stress led to the accumulation of abscisic acid (ABA), jasmonic acid (JA), and salicylic acid (SA) levels, triggering signal transduction events regulated by phosphorylated proteins to improve salt tolerance for *L. barbarum* in saline environments. The phosphorylation of MAPK signaling pathway-related proteins is triggered by reactive oxygen species (ROS) and ABA as signal molecules to induce the expression of downstream salt stress response factors. This study provides a foundation for further analysis of the molecular regulatory mechanism of protein phosphorylation in *L. barbarum* for salt stress.

Keywords *L. barbarum*, Salt stress, Phosphoproteomic, Differentially phosphorylated protein, Glycolysis, Signal transduction

[†]Wangli Liang and Zheng Zhang contributed equally to this work.

*Correspondence:

Lingxia Wang

lxwang@nxu.edu.cn

Wenyu Liang

liang_wy@nxu.edu.cn

¹ School of Life Sciences, Ningxia University, Yinchuan, Ningxia 750021, China

² College of Forestry and Prataculture, Ningxia University, Yinchuan, Ningxia 750021, China

³ State Key Laboratory of Efficient Production of Forest Resources, Yinchuan 750001, Ningxia, China

Introduction

Soil salinity is a major environmental factor limiting plant growth and crop productivity, and its impact is exacerbated by global climate change. Rising levels of soil salinization are projected to affect more than 40% of agricultural land in the coming decades [1, 2]. Excessive accumulation of soluble salts, particularly sodium chloride (NaCl), disrupts the ionic balance in plants, triggering osmotic stress, ion toxicity, and oxidative stress. These changes impair water-use efficiency, alter membrane permeability, transpiration rates, and the growth of



tissues and organs [3, 4]. Notably, salt stress can promote Ca^{2+} signaling and ROS accumulation, alter plant hormone levels and other co-regulatory effects, causing multilevel damage and exacerbating the negative effects of salt stress on plants [5–7]. To mitigate salt stress, plants exhibit dynamic adjustments in regulating growth and survival strategies, although this often comes at the cost of growth potential and productivity [8]. Therefore, there is an urgent need to understand the molecular mechanisms underlying plant responses to salt stress.

Protein phosphorylation is central to plant signal transduction and enzyme regulation, and it dynamically modulates energy metabolism and signal transduction to support plant stress responses and survival [9]. Under salt stress, plants tend to reduce energy allocation related to growth and increase energy expenditure to resist adversity [10]. Glycolysis is one of the main pathways through which plants produce energy under hypoxic or stress conditions. Salt stress can phosphorylate proteins related to the glycolysis pathway, altering enzyme activity, so as to optimize the glycolysis process, increase energy production to cope with physiological changes caused by salt stress, and maintain the homeostasis of plant cells under stress [11, 12]. Under salt stress, plants rapidly sense excessive Na^+ in cells, while initiating the MAPK cascade reaction, Ca^{2+} signal, ABA signal transduction, sucrose non-fermenting-1-related protein kinase 2 (SnRK2) core component and ROS clearance mechanisms activate downstream phosphorylation signaling, regulating salt stress response [5, 13]. MAPK signaling pathway rapidly conveys external stimuli, activating specific target protein phosphorylation through the MAPKKK-MAPKK-MAPK cascade to modulate plant stress responses [14]. Salt stress triggers the opening of Ca^{2+} channels on plant membranes, causing rapid Ca^{2+} influx into the cytoplasm and triggering a Ca^{2+} signaling wave [14–16]. Elevated cytosolic Ca^{2+} levels are sensed by various Ca^{2+} -binding proteins, such as calcium-dependent protein kinases (CDPKs) and calmodulin-like proteins (CMLs) [13, 17]. Upon binding to Ca^{2+} , these sensors initiate the MAPK cascade response, phosphorylated CDPKs directly activate the MAPK cascade, regulating the expression of antioxidant genes, the phosphorylation of CML proteins can also initiate MAPK signaling by modulating specific target proteins [18, 19]. Additionally, increased Ca^{2+} concentration can be sensed by calcineurin B-like proteins (CBLs), which phosphorylate CBL-interacting protein kinases (CIPKs) to regulate Na^+/H^+ levels on plasma membrane [20], playing pivotal roles in the plant's response to environmental stress. MAPK signaling pathway is not only closely related to the Ca^{2+} signal, but also interacts with other signal pathways.

It intersects with ABA signaling pathways to coordinate the expression of genes associated with stomatal closure and stress resistance through phosphorylation events [21]. In addition, the MAPK pathway is related to the production and clearance of ROS, and the activity of NADPH oxidase and the production of ROS are regulated by phosphorylation [22]. Specifically, the ABA- H_2O_2 synergy in guard cells, via SnRK2 activation of NADPH oxidase, amplifies the MAPK pathway's role in ABA signaling [23]. ABA also triggers MKK1-MPK6 cascades, promoting H_2O_2 accumulation and stress response activation, including CAT1 expression for H_2O_2 breakdown [24]. Therefore, understanding how protein phosphorylation regulates plant energy metabolism and signal transduction under salt stress conditions can help elucidate the molecular mechanisms of plant salt tolerance and reveal new factors that regulate salt tolerance.

Lycium barbarum is a perennial shrub of the Solanaceae family, and as a fruit tree with important economic and medicinal value, is rich in polysaccharides and amino acid compounds in its fruit, the goji berry, it is commonly used for dietary and medicinal purposes [25–27]. As a well-known halophyte, *L. barbarum* tolerates soil salinity from 0.3% to 0.6%, up to a $9 \text{ g}\cdot\text{kg}^{-1}$ salt limit [28]. However, natural saline soil is complex and changeable, with fluctuating salt levels and frequent co-occurring stressors such as drought and high pH. In highly saline or multi-stressed saline-soil regions, the growth, fruit yield, and quality of *L. barbarum* may be negatively impacted, despite its inherent salt tolerance. Therefore, exploring the physiological, biochemical, and molecular basis of salt tolerance in *L. barbarum*, and improving salt tolerant varieties to better adapt to saline soil, is crucial for increasing yield and quality of goji berry. Salt stress affects the anatomical structure of *L. barbarum* leaves, leading the palisade tissue cellular structure become looser after exposure to elevated salt concentrations [29]. NaCl and alkaline (NaHCO_3) salt stress significantly reduce *L. barbarum* fresh weight, dry weight, plant height, root height, and the ability to balance Na^+ and K^+ , and diminish gas exchange, photosynthetic pigments, and chlorophyll fluorescence [30–32]. Despite these insights, the role of protein phosphorylation in *L. barbarum* is lacking, hindering a full understanding of its response mechanisms to salt stress, especially in the energy metabolism and signal transduction. In this study, we obtained the information on phosphoproteomic by analyzing data of proteins phosphorylation. These findings will enrich our understanding of the mechanism of *L. barbarum* in response to salt stress.

Results

Protein phosphorylation characteristics

To reveal the underlying mechanism, TMT-based phosphoproteomics analysis was used to identify the phosphorylated proteins in response to NaCl stress. The experimental process is shown in Fig. 1A. The 12% sodium dodecyl sulfate polyacrylamide gel (SDS-PAGE) revealed that the protein bands of the four groups of samples were clear, indicating that the protein quality met the experimental requirements and that these protein samples were suitable for downstream molecular biology experiments (Fig. 1B, Fig. S1). The experimental results revealed 2727 phosphorylated proteins, 5258 phosphorylated peptides and 5096 phosphorylation sites, which included 5252 quantifiable phosphorylated peptides and 5091 quantifiable phosphorylation sites on 2725 quantifiable modified proteins (Fig. 1C). To facilitate the analysis of the distribution of protein phosphorylation sites, we performed quantitative statistical analysis of the phosphorylated sites on all identified proteins. Two or more modification sites were distributed on 42.55% of the proteins, 48 modification sites were found on XP_060208229.1 (Fig. 1D, Table S1). The average number of phosphorylated sites occurring per 100 amino acids was 0.5 in all the phosphorylated proteins (Fig. 1E). We also focused on the occurrence of phosphorylation on different amino acids, and the results revealed that the

proportions of Ser/Thr/Tyr (S/T/Y) phosphorylation sites were 84.18%, 15.54% and 0.28%, respectively (Fig. 1F).

Differential phosphorylation analysis

To obtain more detailed information on proteins modified by phosphorylation, we culled 2189 differentially phosphorylated peptides on the basis of expression fold change (FC) (Table S1 shows some important phosphorylated proteins). We also detected 123, 258, and 822 differentially phosphorylated peptides between control (AT, 0 mM NaCl treatment) and BT (100 mM NaCl treatment), CT (200 mM NaCl treatment), and DT (300 mM NaCl treatment) conditions, respectively (Fig. 2A). Furthermore, we compared the upregulation and downregulation of phosphorylated peptides between the groups (Fig. 2B). First, 532 upregulated and 623 downregulated differentially phosphorylated peptides were identified between BT vs AT, 867 upregulated and 1017 downregulated differentially phosphorylated peptides were identified between CT vs AT, and 1221 upregulated and 1299 downregulated differentially phosphorylated peptides were identified between DT vs AT. Moreover, we found that between DT vs AT, there were two differentially phosphorylated peptides with the FC in expression exceeding 10 times (Fig. 2B).

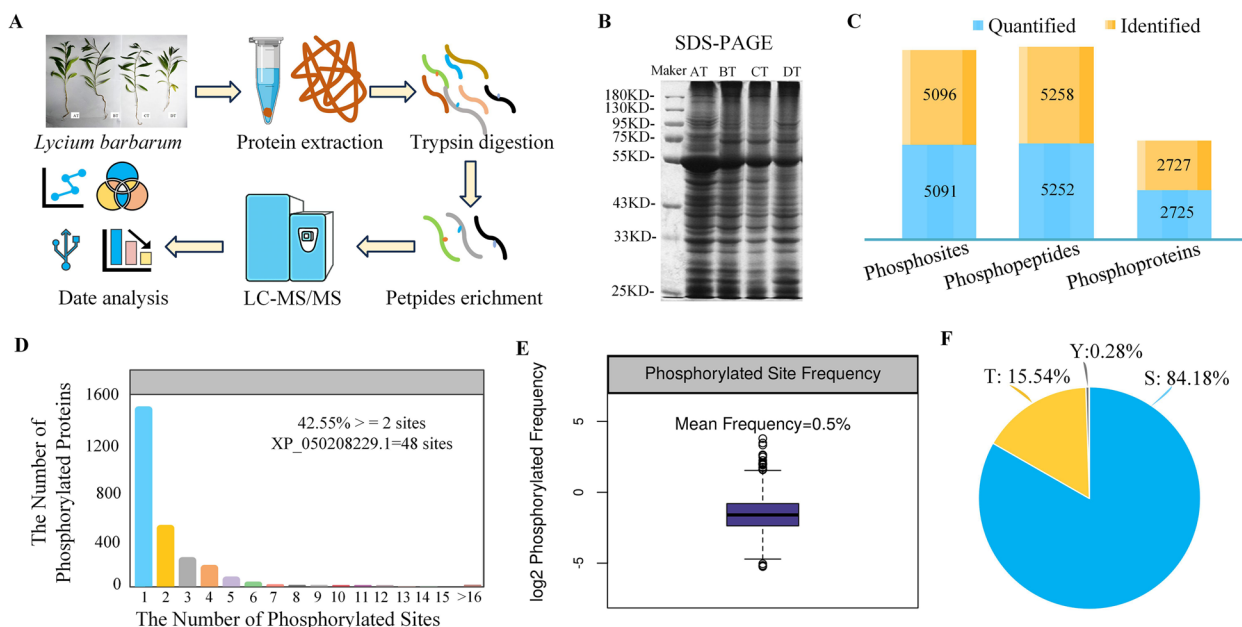


Fig. 1 Global analysis of protein phosphorylation modification of *L. barbarum* in response to NaCl stress. **A** Overview of the analytical workflow; **(B)** SDS-PAGE analysis of proteins; **(C)** The number of phosphorylated proteins and sites; **(D)** Map of the number of phosphorylation sites; **(E)** Distribution frequency diagram of phosphorylation sites; **(F)** Distribution scale diagram of Ser/Thr/Tyr phosphorylation sites. AT. 0 mM NaCl treatment; BT. 100 mM NaCl treatment; CT. 200 mM NaCl treatment; DT. 300 mM NaCl treatment

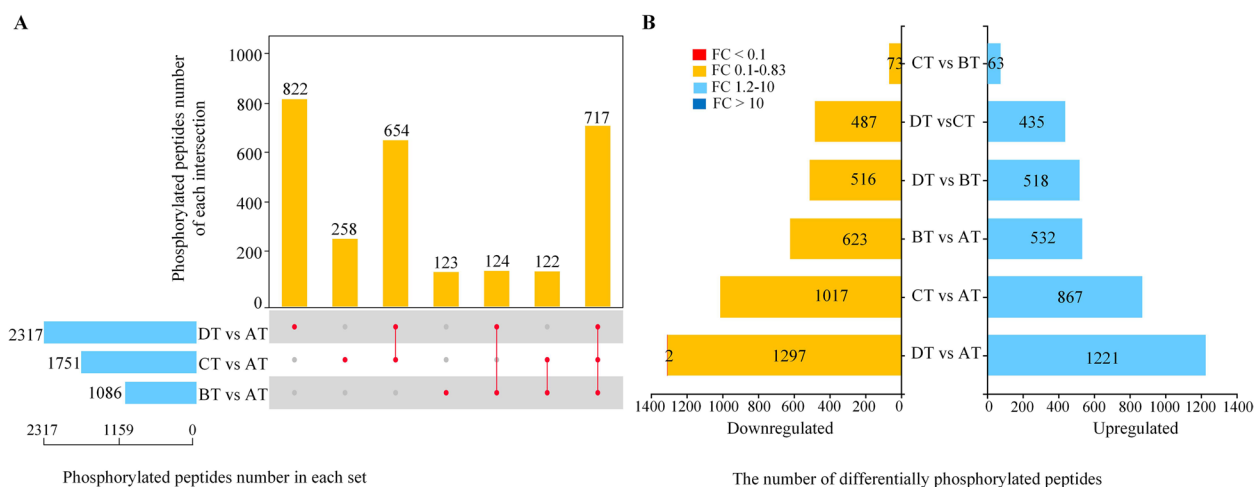


Fig. 2 Differential phosphorylated peptides analysis. **A** Upset figures of identified phosphorylated peptides among the groups sample; **(B)** Histogram of quantitative difference of phosphorylated peptides. AT. 0 mM NaCl treatment; BT. 100 mM NaCl treatment; CT. 200 mM NaCl treatment; DT. 300 mM NaCl treatment

Hierarchical clustering analysis of differential phosphorylated peptides

It is generally believed that proteins with similar expression patterns may have similar functions or play similar regulatory roles in biological pathways. In this study, hierarchical clustering analysis was carried out on the screened differentially phosphorylated peptides (Fig. 3), and the results revealed that the differentially phosphorylated peptides were divided into two clusters, with increasing NaCl stress, cluster I was upregulated, and cluster II was downregulated (Fig. 3). A comparison of the 0 mM NaCl treatment with the 100, 200 and 300 mM NaCl treatments revealed that there were obvious distinctions between the different groups and good intragroup repeatability (Fig. 3A, B and C).

Functional analysis of DEPPs

To thoroughly understand the functions and characteristics of the differentially phosphorylated proteins (DEPPs) in *L. barbarum* under salt stress, we explored the gene ontology (GO), kyoto encyclopedia of genes and genomes (KEGG) pathway and protein–protein interaction (PPI) analyses of the DEPPs corresponding to the differentially phosphorylated peptides shown in Fig. 2. To predict the molecular regulatory mechanism, GO was used to study the functional annotation of DEPPs in the three branches, and the significantly enriched GO terms reflected the multifaceted biological activities of the cells (Fig. 4A, B and C, Table S2). Comparison of the 0 mM NaCl and 100 mM NaCl treatments showed that DEPPs were significantly enriched in key biological processes

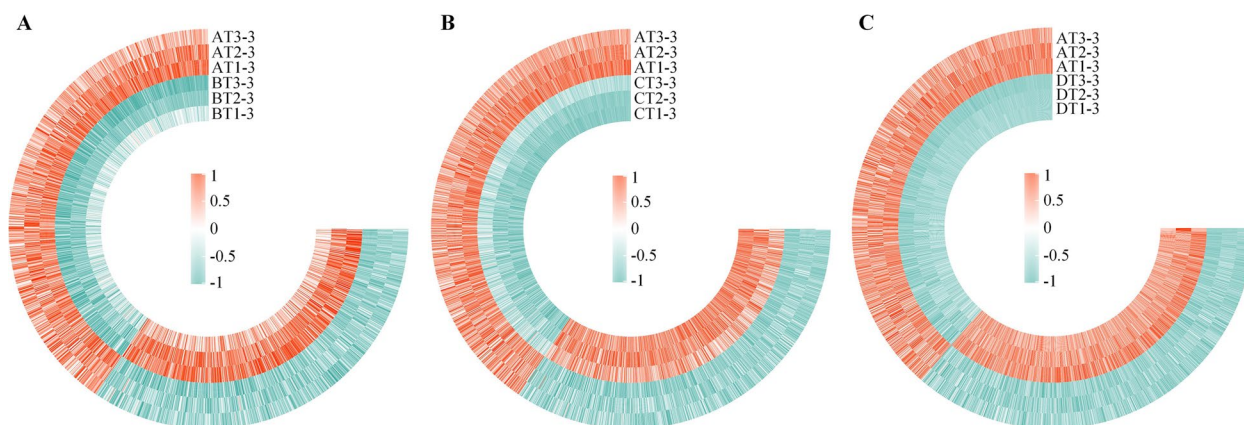


Fig. 3 Cluster analysis of differentially phosphorylated peptides expression patterns in *L. barbarum* under NaCl stress. **A** BT vs AT; **(B)** CT vs AT; **(C)** DT vs AT. AT. 0 mM NaCl treatment; BT. 100 mM NaCl treatment; CT. 200 mM NaCl treatment; DT. 300 mM NaCl treatment

(Fig. 4A), such as various nucleoside triphosphate metabolic processes (86), RNA splicing (25), RNA processing (24), response to lipids (18), ATP metabolism (15), mRNA

processing (11), leaf development (7), and cell death (5). They may participate in regulatory molecular functions, including symporter activity (10), glucose and hexose

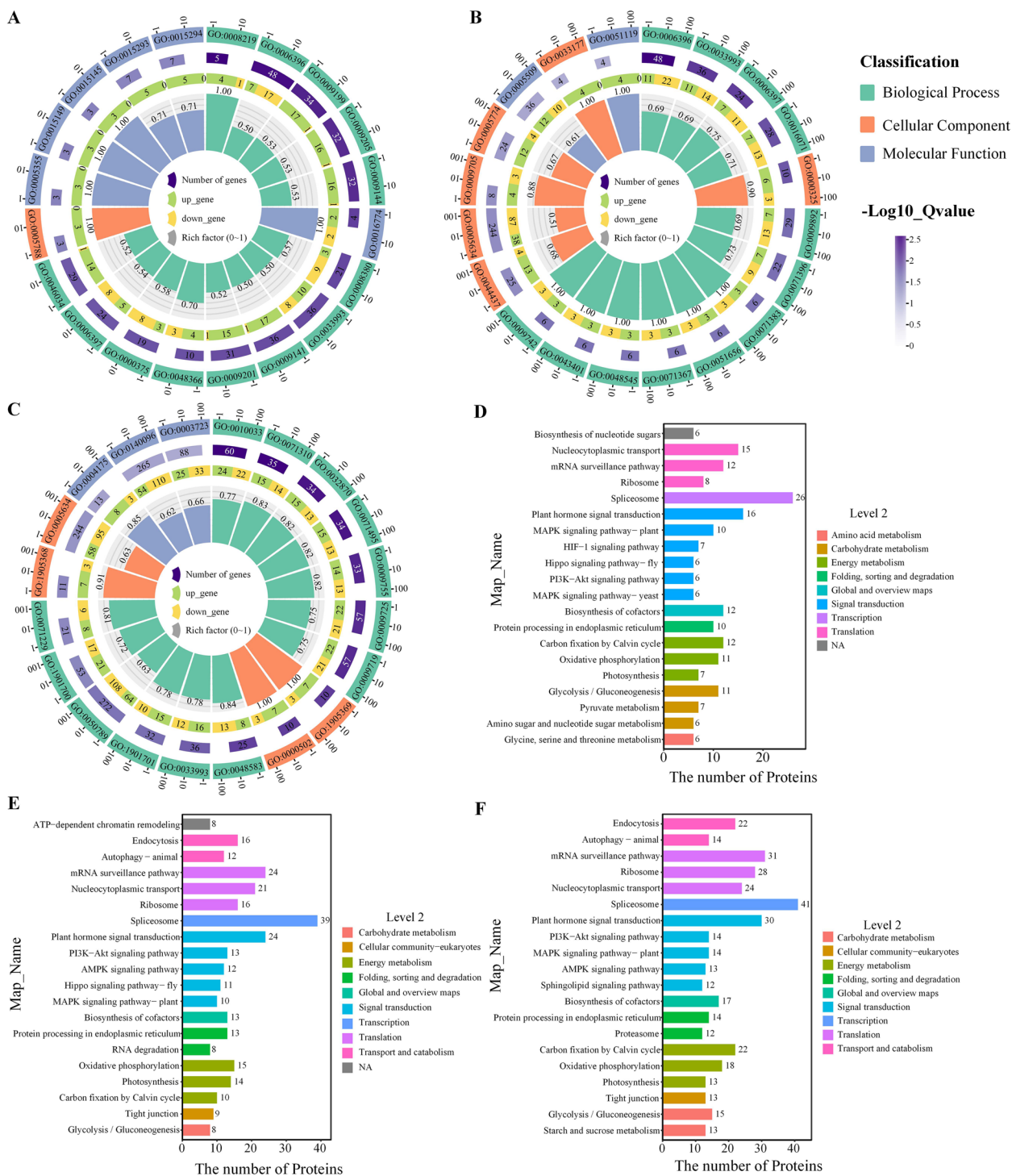


Fig. 4 GO and KEGG pathway annotation of DEPPs in *L. barbarum* under NaCl stress. **A** and **(D)** BT vs AT; **(B)** and **(E)** CT vs AT; **(C)** and **(F)** DT vs AT. AT. 0 mM NaCl treatment; BT. 100 mM NaCl treatment; CT. 200 mM NaCl treatment; DT. 300 mM NaCl treatment

transmembrane transport (9), and phosphotransferase activity with carboxyl group acceptors (4), among others. Additionally, certain DEPPs were integral components of the endoplasmic reticulum lumen (3). In the comparison of the 0 mM and 200 mM NaCl treatments (Fig. 4B), the greatest number of DEPPs were involved in response to lipids (41) and hormone-mediated signaling pathways (30). Some DEPPs also participated in RNA processing (33), mRNA metabolic process (20), mRNA processing (18), organelle localization (6), and other metabolic processes (20). In terms of molecular functions, DEPPs contributed mainly to calcium ion binding (22) and sugar transmembrane transporter activity (4), whereas in the cellular component category, DEPPs were key in nucleus (125), vacuolar part (25), vacuolar membrane (16), plant-type vacuole membrane (7), proton-transporting two-sector ATPase complex (4). Similarly, in the comparison of the 0 mM and 300 mM NaCl treatment groups (Fig. 4C), DEPPs were significantly involved in biological processes such as responses to organic substances (75), hormone stimuli (71), endogenous stimuli (71), oxygen-containing compounds (63), hormone-mediated signaling (27), regulation of responses to stimuli (21), responses to lipids (28) and acid chemicals (17) and other biological process (172). In terms of molecular functions, DEPPs were associated primarily with binding and transport activities (233), whereas in terms of cellular components, they were related to regulating nuclear function and protein-containing complexes (183).

KEGG pathway enrichment analysis of the DEPPs revealed several significantly enriched biological pathways ($p < 0.05$), suggesting potential functional roles in the underlying cellular processes. The top 20 KEGG pathways, with the greatest number of DEPPs, between the 0 mM NaCl and 100, 200 and 300 mM NaCl treatments were identified and are shown in Fig. 4D, E and F, Table S2. In the comparison of the 0 mM NaCl and 100 mM NaCl treatments, the top enriched pathways were the spliceosome (26), plant hormone signal transduction (16), and nucleocytoplasmic transport pathways (15), indicating a strong association with posttranscriptional regulation and intracellular communication. Additionally, pathways involved in mRNA surveillance (12), biosynthesis of cofactors (12), and carbon fixation via the Calvin cycle (12) were strongly represented, highlighting the involvement of metabolic and regulatory networks. Key energy-related pathways, such as glycolysis/gluconeogenesis (11) and oxidative phosphorylation (11), were also enriched, suggesting shifts in metabolic activity in response to the experimental conditions. Finally, significant enrichment was observed in the MAPK signaling pathway in plants (10) and protein processing in the endoplasmic reticulum (10), indicating alterations

in the stress response and protein folding mechanisms (Fig. 4D). Upon comparing the 0 mM NaCl treatment with the 200 and 300 mM NaCl treatments, we identified several significantly enriched pathways at the second hierarchical level in the KEGG classification, and the pathways related to carbohydrate metabolism, energy metabolism, and signal transduction were strongly represented, suggesting metabolic shifts and altered intracellular signaling processes. Enrichment was also observed in pathways associated with cellular community eukaryotes, folding, sorting, degradation, transport and catabolism, indicating modifications in cellular organization and protein quality control (Fig. 4E and F). Notably, we focused on the significantly enriched pathways of DEPPs involved in the response to salt stress in *L. barbarum*, including those related to glycolysis, the MAPK signaling pathway-plant and plant hormone signal transduction (Fig. 4). These results suggest that phosphorylation may regulate an array of proteins associated with energy metabolism, signal transduction and other biological processes in *L. barbarum* under salt stress.

Building on the GO and KEGG pathway analyses, a PPI network was constructed, with a focus on signal transduction pathways and glycolysis. Through this PPI analysis, we identified several key nodes that play crucial roles in the response of *L. barbarum* to salt stress. The phosphorylated proteins at these nodes were predominantly associated with the glycolysis pathway, plant hormone and MAPK signal transduction processes, Cluster I represented glycolysis, Cluster II represented plant hormone signal transduction, and Cluster III represented MAPK signal transduction (Fig. 5, Table S1). This intricate network helped *L. barbarum* maintain their metabolic balance, and had a certain degree of influence on the physiological response to salt stress, but the exact mechanism of action and the degree of influence remain to be further studied.

Parallel reaction monitoring (PRM) analysis

To validate the expression trends of differentially phosphorylated proteins and the reliability of the TMT-based phosphoproteomics results. The DEPPs XP_060207004.1, XP_060173866.1, XP_060171813.1, XP_060171737.1, XP_060196372.1 and XP_060205343.1 in Table S1 were verified via PRM. The PRM results confirmed the expression patterns observed in the initial analysis, with strong consistency in the fold-change values between the PRM data and the phosphoproteomic results (Fig. 6, Table S1, Fig. S2). The high concordance between the PRM and TMT phosphoproteomic results strengthened the reliability of the protein identification results and the predicted associations with key stress response pathways. This targeted validation highlighted the pivotal role of

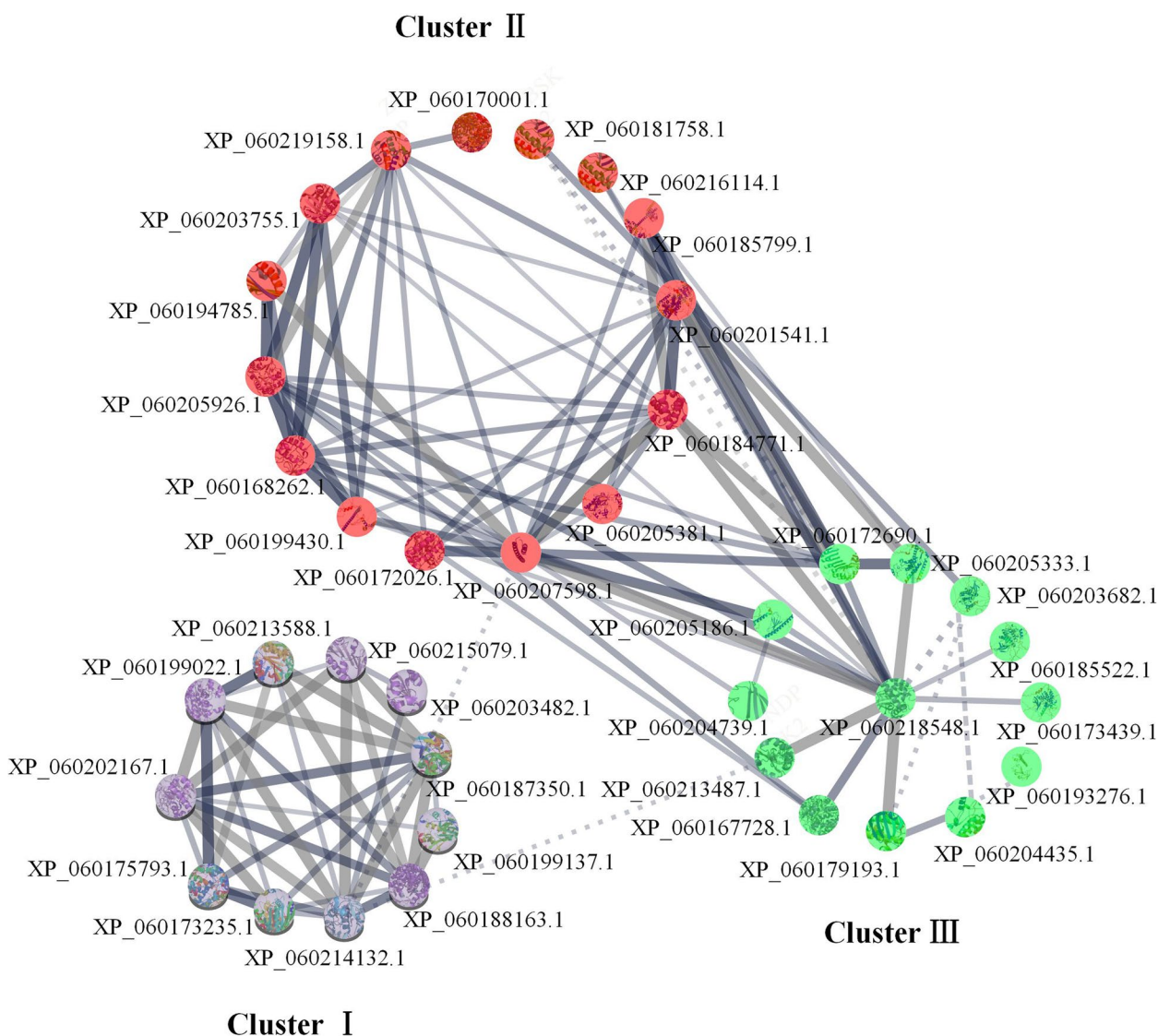


Fig. 5 Protein–protein interaction networks of DEPPs involved in energy metabolism and signal transduction pathway in *L. barbarum* under NaCl stress. Each node in the graph represents a phosphorylated protein, these phosphorylated proteins are listed in Table S1, and line thickness indicates the strength of data support. Network is clustered to 3 clusters, which are represented with red, green and purple nodes, respectively

phosphorylation-mediated regulation in the adaptation of *L. barbarum* to salt stress.

Changes in enzyme activity

As salt stress intensified, the activities of glycolysis enzymes fructose-1,6-diphosphate aldolase (FBA), triosephosphate isomerase (TPI) and 3-phosphoglycerate kinase (PGK) decreased at first and then recovered, with the lowest activities observed under 200 mM NaCl treatment (Fig. 7B-D). In contrast, the activities of 1,6-diphosphofructosase (FBPase) and acetyl-CoA carboxylase (ACC) continuously decreased with increasing NaCl concentration and reached their minimum values

under 100 mM and 300 mM NaCl treatment, respectively (Fig. 7A, F). Moreover, compared with that in the control (0 mM NaCl), pyruvate dehydrogenase E1 component subunit alpha (PDHA) activity, which is associated with pyruvate metabolism, significantly increased under all the salt stress conditions (Fig. 7E). These findings provide crucial insights into the regulatory mechanisms of glycolysis and pyruvate metabolism under salt stress.

Changes in the levels of various substances

As the NaCl concentration increased, the glucose content in *L. barbarum* markedly increased, peaking under

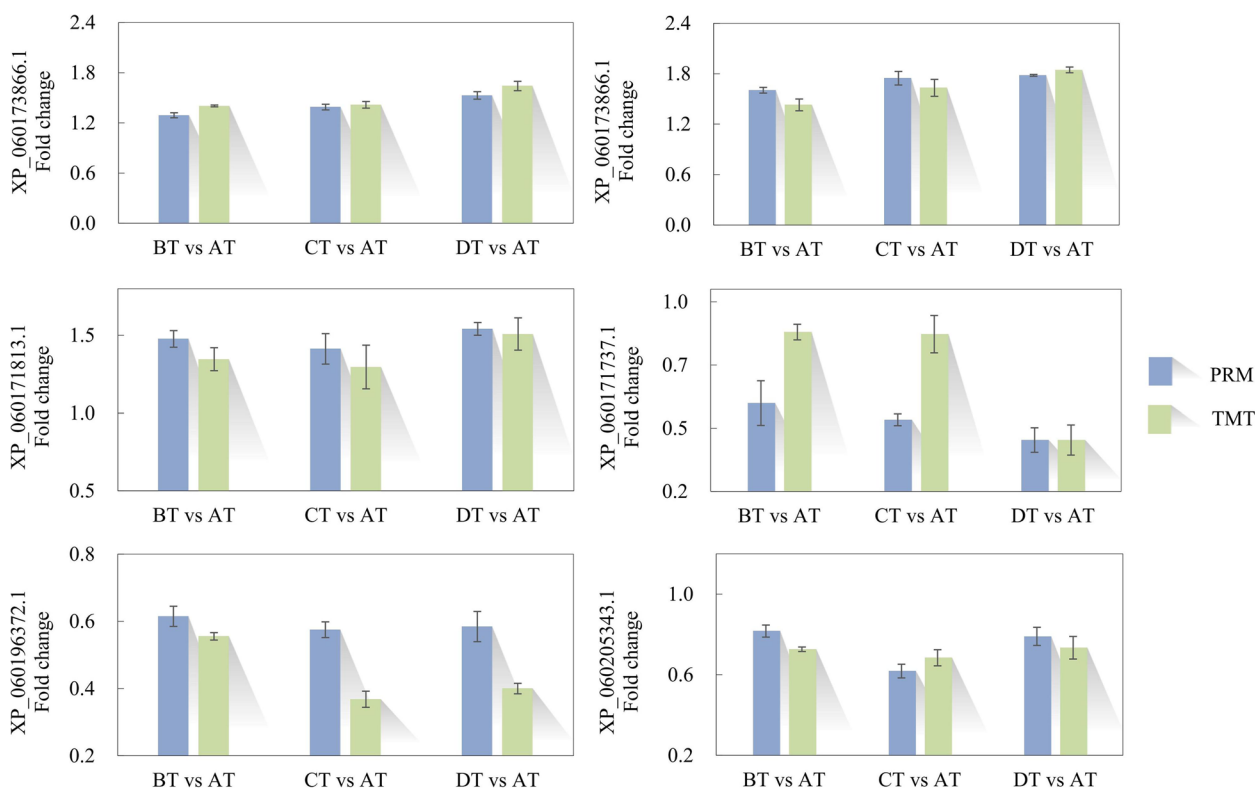


Fig. 6 PRM analysis of phosphorylated proteins of *L. barbarum* under NaCl stress. AT. 0 mM NaCl treatment; BT. 100 mM NaCl treatment; CT. 200 mM NaCl treatment; DT. 300 mM NaCl treatment

200 mM NaCl treatment (Fig. 8A). Concurrently, the levels of oxidized nicotinamide adenine dinucleotide (NAD⁺) decreased (Fig. 8B), whereas the levels of reduced nicotinamide adenine dinucleotide (NADH) significantly increased (Fig. 8C), indicating metabolic reallocation and adjustment within plant cells under high-salt conditions. Under 200 mM and 300 mM NaCl stress, the ABA content was notably greater than that in the control (Fig. 8D), suggesting that increased ABA accumulation is a key regulatory response that enhances salt tolerance. In response to NaCl stress, the JA, 12-oxo-phytodienoic acid (OPDA), jasmonyl isoleucine (JA-ILE) and dihydrojasmonic acid (2HJA) levels obviously changed (Fig. 8E-H). Under 100 mM NaCl treatment, the contents of these compounds sharply decreased, indicated that *L. barbarum* preferentially activated other physiological mechanisms to cope with stress (Fig. 8E-H). However, as the NaCl concentration increased to 200 and 300 mM, the levels of these compounds began to rise, reflecting the compensatory mechanisms of the plants to cope with strong salt stress. Notably, the JA and OPDA contents in the 300 mM NaCl treatment group were almost equivalent to those in the control group (Fig. 8E and F), suggesting a degree of homeostatic regulation. In contrast, the JA-Ile and 2HJA levels were significantly greater than

those in the salt-free treatment, indicating their pivotal roles in regulating stress responses under high-salt conditions (Fig. 8G and H). Under NaCl stress, the level of SA increased (Fig. 8I). SA functions as a signaling molecule that mediates the plant's stress response by activating defense mechanisms to increase stress adaptation. The H₂O₂ content significantly increased with the increasing NaCl concentration (Fig. 8J), indicating that NaCl stress triggered an oxidative stress response in *L. barbarum* cells. This coordinated shift in metabolic pathways underscores the intricate regulation through energy conversion and signaling for adaptation to salt stress (Fig. 8).

Discussion

L. barbarum is a fruit tree of significant economic value that is widely cultivated for its fruit, the goji berry, which is rich in nutrients and has medicinal properties. However, in the context of global climate change and increasing soil salinization, salt stress has emerged as a major factor that negatively affects seedling growth and goji berry yield and quality. As a halophytic plant, *L. barbarum* possesses a certain level of salt tolerance, but enhancing its ability to withstand salt stress remains of practical importance. In recent years, research on the salt tolerance mechanism of *L. barbarum* has garnered

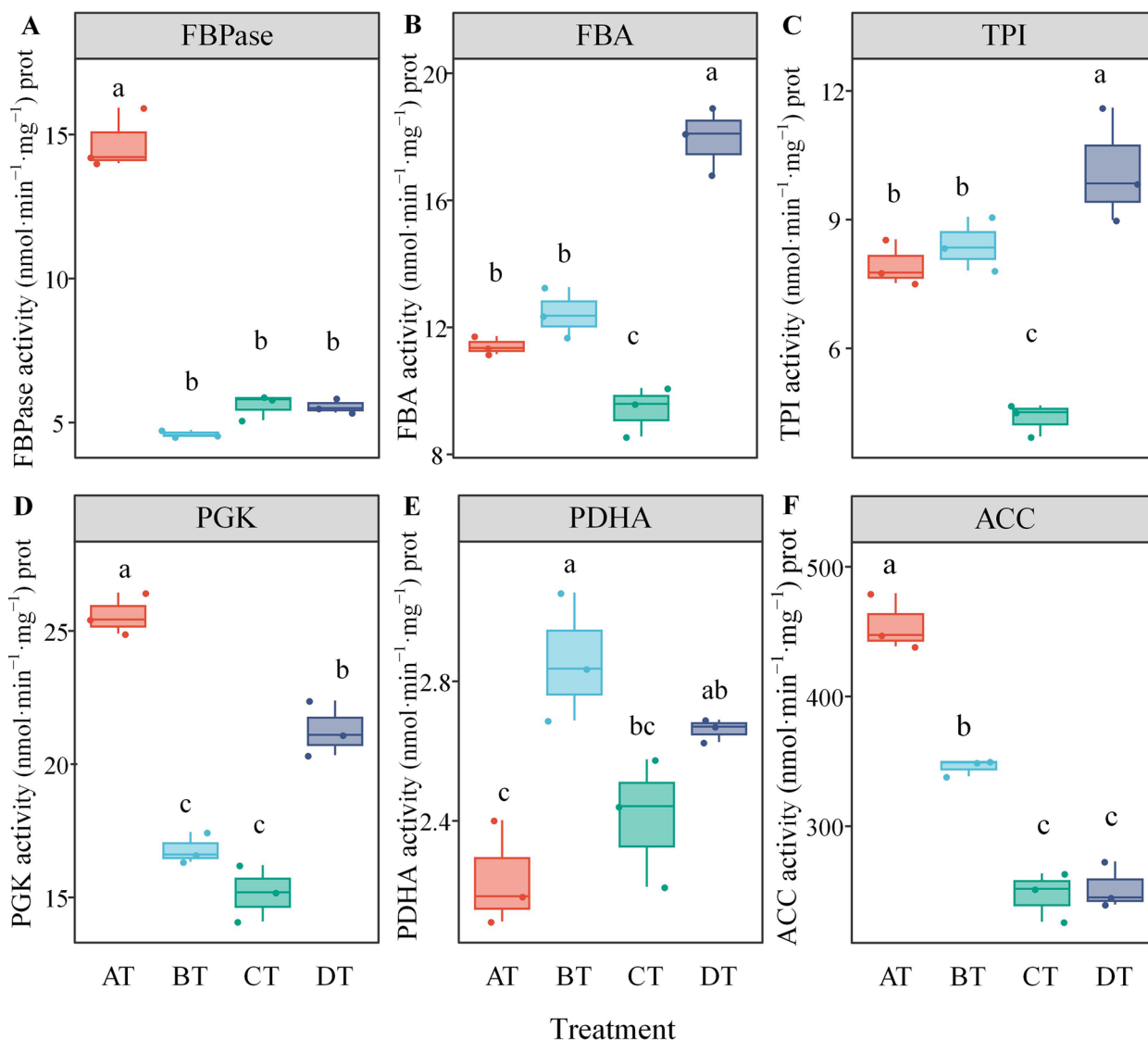


Fig. 7 The changes of the key enzyme activity of *L. barbarum* under NaCl stress. **A** FBPase activity; **B** FBA activity; **C** TPI activity; **D** PGK activity; **E** PDHA activity; **F** ACC activity. AT, 0 mM NaCl treatment; BT, 100 mM NaCl treatment; CT, 200 mM NaCl treatment; DT, 300 mM NaCl treatment. The data are presented as the means \pm SE of three replicates. The different lowercase letters between groups indicate significant differences ($p < 0.05$)

increasing attention, with a particular focus on its morphological and physiological responses to salt stress [29, 31]. In this study, a total of 2189 differentially phosphorylated peptides were identified in response to NaCl stress. We focused on two main functions: glycolysis and signal transduction pathways. Among them, the glycolysis, ABA, JA and MAPK signal transduction pathways were the main regulatory pathways (Fig. 9). These results will help us to further study the salt tolerance of *L. barbarum*.

Protein phosphorylation regulates glycolysis in *L. barbarum* in response to NaCl stress

The phosphorylation of glycolytic proteins plays a crucial role in regulating energy production and generating intermediate metabolites essential for plant development and stress responses. Fructose can be converted to fructose 6-phosphate (F6P) through one-step catalysis by fructokinase (FRK) and enter glycolysis, glucose-6-phosphate isomerase (GPI), FBPase and phosphofructokinase (PFK) are important enzymes in glycolysis, which can catalyze the interconversion of glucose-6-phosphate,

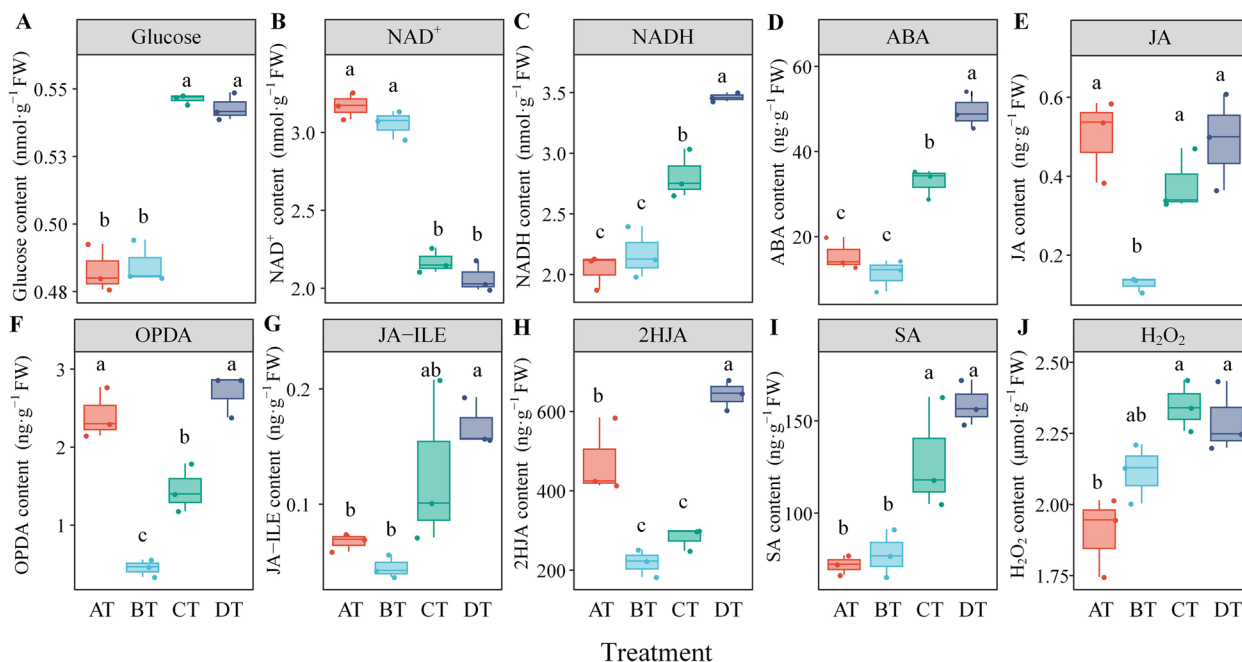


Fig. 8 The changes of the key substance contents of *L. barbarum* under NaCl stress. **A** Glucose content; **B** NAD⁺ content; **C** NADH content; **D** ABA content; **E** JA content; **F** OPDA content; **G** JA-ILE content; **H** 2HJA content; **I** SA content; **J** H₂O₂ content. AT, 0 mM NaCl treatment; BT, 100 mM NaCl treatment; CT, 200 mM NaCl treatment; DT, 300 mM NaCl treatment. The data are presented as the means ± SE of three replicates. The different lowercase letters between groups indicate significant differences ($p < 0.05$)

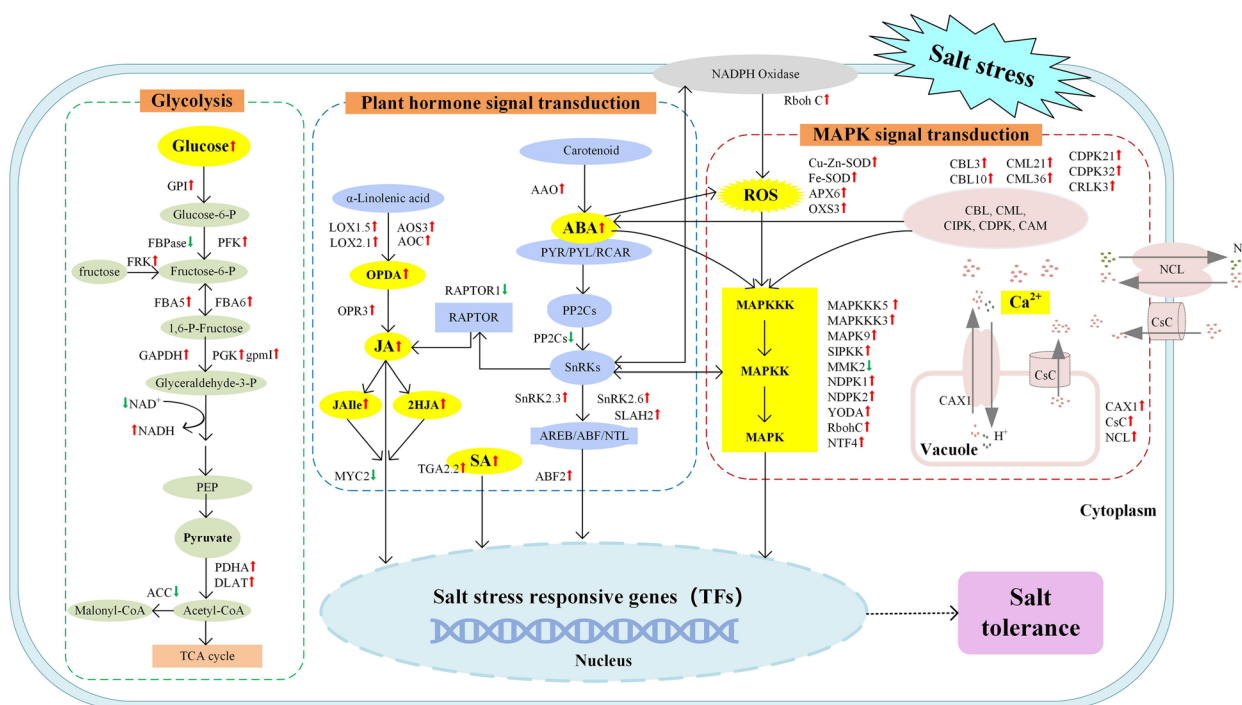


Fig. 9 Regulation network map of glycolysis and signal transductions participate in *L. barbarum* in response to NaCl stress through protein phosphorylation. The proteins with increased phosphorylation are shown in red arrow, proteins with decreased phosphorylation are shown in green arrow

fructose-1,6-diphosphate and F6P, thus adjusting the metabolic flow of the glycolysis and gluconeogenesis and providing cells with more energy and raw materials required for synthetic metabolism [33]. PFK, the rate-controlling enzyme in glycolysis, is activated through S/TPK-catalyzed phosphorylation [11, 34]. In *Pyropia haitanensis*, the phosphorylation sites of PFK are enriched under sustained high-temperature stress, which promotes the tolerance of this species to heat stress [35]. High glucose levels in plants activate PFK and inhibit FBPase, promoting glycolysis and reducing gluconeogenesis [36]. Our findings revealed that salt stress in *L. barbarum* led to a rapid glucose accumulation, increased phosphorylation of FRK2, GPI and PFK, decreased FBPase phosphorylation and activity, indicating that *L. barbarum* enhanced its glycolysis pathway in saline environments, effectively utilizing glucose for energy production and reducing unnecessary gluconeogenesis (Table S1, Fig. 8A, Fig. 7A). Under 200 mM NaCl stress, the activities of FBA and TPI decreased, indicating that the associated metabolic processes were hindered. In 300 mM NaCl environment, the high levels of phosphorylation of FBA5 and FBA6, along with increased enzyme activities of FBA and TPI, suggested that *L. barbarum* strived to maintain necessary energy supply and metabolic balance in response to this high-salt induced stress (Table S1, Fig. 7B and C). Glyceraldehyde 3-phosphate is subsequently oxidized by glyceraldehyde 3-phosphate dehydrogenase (GAPDH) to 1,3-diphosphoglycerate, and this transformation is accompanied by the reduction of NAD⁺ to NADH, GAPDH is closely associated with the process of plant response to stress, the increased phosphorylation level of GAPDH in refrigerated tomato fruit indicates the activation of cold stress signals [37, 38]. We observed that with increasing phosphorylation of GAPDH in *L. barbarum* under high NaCl stress, the NAD⁺ content decreased and the NADH content increased, which further confirmed the acceleration of glycolysis metabolism, and these metabolic alterations strongly suggested that glycolytic metabolism is accelerated in response to stressful environmental conditions (Table S1, Fig. 8B, C). PGK can convert 1,3-diphosphate to 3-phosphate, which is crucial for the stress tolerance of plants [39]. In *L. barbarum*, as NaCl stress increased, the phosphorylation level of PGK increased, whereas its activity initially decreased but then increased, these changes in phosphorylation and activity levels were closely associated with the production of 3-phosphoglycerate (Table S1, Fig. 7D). Similarly, phosphoglycerate mutase (gpm1) exhibited significant phosphorylation under NaCl stress (Table S1), causing glycolysis to shift towards pyruvate production. Pyruvate dehydrogenase complexes (PDHs) can convert pyruvate to acetyl-CoA,

which is mainly responsible for carbon atoms entering the tricarboxylic acid (TCA) cycle [40]. The function of ACC is to convert acetyl-CoA to malonyl-CoA, and leads a decrease in the flow rate affects the activity of the TCA cycle [41]. In *L. barbarum*, NaCl stress induces a rise in phosphorylation of PDHA and dihydrolipoyllysine-residue acetyltransferase component 2 of the pyruvate dehydrogenase complex (DLAT), and a decline in ACC phosphorylation and activity (Table S1), which may increase the generation of acetyl-CoA and promote the TCA cycle under NaCl stress, indicating that sufficient acetyl-CoA levels are maintained to ensure utilization and metabolic flux in the TCA cycle (Table S1, Fig. 7F). NaCl stress induced the phosphorylation of proteins involved in glycolysis, and the accelerated transformation of intermediate metabolites suggested that the efficiency of glycolysis significantly improved (Fig. 9). This may serve as a compensatory mechanism to maintain cellular energy homeostasis under high NaCl stress.

Protein phosphorylation regulates plant hormone signal transduction in *L. barbarum* in response to NaCl stress

Under salt stress, the ABA content of some salt-tolerant plants tends to stabilize, but as the stress level increases, the ABA content rapidly increases [42], and ROS and Ca²⁺ signals under salt stress can promote rapid accumulation of ABA within a few hours of stress [7]. The significant changes in the phosphorylation levels of violaxanthin de-epoxidase (VDE) and abscisic aldehyde oxidase (AAO) in *L. barbarum* under salt stress may enhance their enzymatic activities, leading to a rapid increase in endogenous ABA levels, we also found that 200 mM and 300 mM NaCl significantly indeed elevated ABA content in *L. barbarum*, suggesting that ABA signaling plays a crucial role in the response to salt stress (Table S1, Fig. 8D). When the ABA receptor pyrabactin resistance/regulatory component of ABA receptor (PYR/PYL/RCAR) perceives ABA molecules, it interacts with its co-receptor protein phosphatase 2C (PP2C) and inhibits PP2C phosphatase activity, thereby relieving the inhibitory effect of PP2C on the key positive regulatory factor SnRK2 kinase in the ABA signaling pathway, SnRK2 can phosphorylate and activate response factors of a series of ABA signaling pathways, and ABA mediated ABA responsive element AREB/ABRE binding factors (ABFs) phosphorylation is necessary for activating ABA responsive genes [21, 42]. Our findings supported this explanation, suggesting that ABA accumulation, and the decreased phosphorylation levels of PP2C 16 and other PP2C proteins, promote increased phosphorylation levels of SnRK2.3 and SnRK2.6, thereby activating the ABA signaling pathway and stress response process under salt stress (Table S1, Fig. 8D). The significant phosphorylation

of ABF2 (bZIP46) in *L. barbarum* under high-salt conditions indicates a positive response of downstream components in the ABA signaling pathway to salt stress (Table S1). In addition, the activated SnRK2 protein kinase OST1 (SnRK2.6) directly binds to and phosphorylates the S-type anion channel SLAC1 (SLAC1), thereby promoting stomatal closure to reduce water loss in saline environments [22, 43]. Additionally, under abiotic stress, OST1 phosphorylates reduced nicotinamide adenine dinucleotide phosphate oxidase (NADPH oxidase) [22, 44], OST1 and ROS activate calcium channels, increase the Ca^{2+} concentration [45]. We discovered that ABA accumulation promoted the phosphorylation of OST1 and induced stomatal closure and ROS signal generation through the phosphorylation of SLAH2 and NADPH oxidase respiratory burst oxidase homolog protein C (Rboh C), and the activation of Ca^{2+} channels enabled ABA feedback regulation (Fig. 8, Table S1). Importantly, the signaling pathway coupled with the plant target of rapamycin (TOR) kinase and ABA receptor is regulated by phosphorylation, under abiotic stress, ABA activated SnRK2 kinase phosphorylates TOR kinase 1B (RAPTOR1B) to inhibit TOR kinase activity and growth inhibition [6, 46]. It is hypothesized that the enriched ABA signal inhibited RAPTOR1 phosphorylation and TOR kinase activity, helping *L. barbarum* save energy in unfavorable environments. Briefly, the enhanced ABA signal may promote the adaptability of *L. barbarum* in salt environment (Table S1, Figs. 8D, J and 9).

The activation of the lipoxygenase (LOX) pathway initiates the biosynthesis of JA and its derivatives, including OPDA, JA-Ile, and 2HJA. OPDA and JA regulate gene expression, enhance the plant antioxidant system, and maintain osmotic balance [8, 47]. JA-Ile primarily regulates stress responses, whereas 2HJA enhances salt tolerance through complex mechanisms [47, 48]. Salt stress increases JA levels in leaves and roots, enhances the activity of the antioxidant system to neutralize excess ROS, OPDA triggers the expression of stress-related genes, and the broader JA-JA-Ile network supports salt tolerance [47, 48]. In this study, salt stress increased the phosphorylation of lipoxygenase 1.5 (LOX1.5), lipoxygenase 1.2 (LOX1.2), allene oxide synthase (AOS), allene oxide cyclase (AOC), and 12-oxophytodienoate reductase 3 (OPR3), and promoted the accumulation of JA, OPDA, JA-Ile and 2HJA (Table S1, Fig. 8E-H). These findings suggest that salt stress adjusts the hormone balance in *L. barbarum* by regulating key enzyme activities through phosphorylation. Initially, the JA and OPDA levels decreased as a resource-saving strategy but later recovered as the plant acclimated, JA-Ile and 2HJA levels increased under relatively high salt concentrations, reflecting strengthening of the stress response, which

helped *L. barbarum* adapt and maintain homeostasis (Fig. 8G and H). In plant growth regulation by JA signal transduction, an autoregulatory negative feedback loop is formed by the transcription factor MYC2 (MYC2) and bHLH transcription factor MTB (MTB) to terminate the JA signal, MTB competes with MYC2 for binding to target gene promoters, and continuous MYC activation by JA inhibits plant growth [49]. Mutations in the MYC2 phosphorylation site lead to obstruction of JA signal transduction [49, 50]. In *L. barbarum*, salt stress decreased the phosphorylation levels of MYC2 and MTB1 (Table S1), preventing continuous activation of MYC proteins and indicating that the JA signaling pathway was regulated. In addition, mutation of *RAPTOR1B* reportedly leads to a significant decrease in the levels of JA, JA-Ile, and OPDA [51]. We observed a decrease in the jasmonate content in response to 100 mM NaCl, which may be closely related to the decrease in the RAPTOR1 phosphorylation level in *L. barbarum* under salt stress (Table S1). In essence, *L. barbarum* reduced the damage caused by excessive activation of the JA signaling pathway by adjusting the jasmonate content under salt stress conditions (Table S1, Figs. 8E-H and 9).

SA can alleviate the impact of salt stress by inducing the expression of stress-related genes, activating antioxidant defense systems, regulating ion absorption and distribution, and interacting with other hormones or signaling molecules [8]. As the salt concentration increased, *L. barbarum* initiated defense responses by synthesizing and accumulating more SA, which may also regulate a series of physiological and biochemical reactions, further research is needed to confirm this (Fig. 8I). Under stress, acid receptors NPR1 (NPR1) interacts with transcription factor 2.2 (TGA2.2) to activate *PR* gene transcription, enhancing SA signaling and increasing plant defense [52]. Salt stress increased TGA2.2 phosphorylation in *L. barbarum*, suggesting that this phosphorylation may regulate TGA2.2 activity (Table S1, Fig. 9), promoting *PR* gene activation and thereby improving salt stress tolerance.

Protein phosphorylation regulates the MAPK signaling pathway in *L. barbarum* in response to NaCl stress

The MAPK signaling pathway can transmit stress signals to the nucleus via a kinase phosphorylation cascade, thereby regulating ion balance, osmotic pressure, and shielding cells from oxidative stress with antioxidants [14, 53]. Salt stress led to the opening of Ca^{2+} channels on plant membranes and the formation of intracellular Ca^{2+} signaling wave [14–16]. Under salt stress, the phosphorylation of sodium/calcium exchanger NCL (NCL), calcium permeable stress-gated cation channel 1-like (CsC1), and vacuolar cation/proton exchanger 2-like (CAX2) may lead to a transient increase in cytoplasmic

Ca²⁺ and trigger downstream signals in *L. barbarum* (Table S1, Fig. 9). Our results revealed that the salt adaptability of *L. barbarum* was regulated by the phosphorylation of multiple calcium-binding proteins (Table S1, Fig. 9). Upon sensing an increase in intracellular Ca²⁺, these proteins likely interact with key molecules in the MAPK pathway through phosphorylation, thereby playing a role in the stress response of *L. barbarum* (Fig. 9). Future research should focus on the specific positioning and mechanism of action of these proteins in the MAPK cascade to reveal the stress regulatory network.

H₂O₂, a key environmental adaptation signal, rose significantly in *L. barbarum* cells under salt stress, along with increased phosphorylation of antioxidant enzymes like [Cu–Zn] (Cu–Zn-SOD), superoxide dismutase [Fe] (Fe-SOD), L-ascorbate peroxidase 6 (APX6), and oxidative stress 3 (OXS3) also increased (Fig. 8J), Table S1), indicating that salt stress regulated the activity of antioxidant enzymes through phosphorylation, helping *L. barbarum* withstand ROS-induced oxidative stress. ROS signaling is intertwined with MAPK signaling, with ROS activating MAPK and the MAPK cascade regulating the dynamic balance of ROS [5, 53]. Rboh-dependent H₂O₂ production is crucial for plant stress tolerance, and MPK8 negatively regulates ROS by controlling *RbohD* expression [54]. Salt and drought stress upregulate *RbohC* and *RbohF*, enhancing NADPH oxidase activity and H₂O₂ generation, which forms a feedback loop by further inducing *RbohC* and *RbohF* expression [55]. In MAPK signal transduction, mitogen-activated protein kinase kinase SIPK (SIPK) / mitogen-activated protein kinase homolog NTF4 (NTF4) and Mitogen-activated protein kinase kinase SIPKK (SIPKK) / NTF4 induce ROS production, and the MAPK cascade mitogen-activated protein kinase kinase kinase 2 (MEK2)-SIPK/NTF4 participates in the regulation of the radical burst [56]. Under high-salt stress, the phosphorylation levels of *RbohC*, NTF4, and SIPKK significantly increased in *L. barbarum*, we hypothesize that salt stress triggers ROS production, activating the MAPK cascade to amplify signals and regulate defenses like antioxidant systems and stress gene expression (Table S1, Fig. 9). Similarly, nucleoside diphosphate kinase 2 (NDPK2) participates in H₂O₂-mediated MAPK signaling pathways, the overexpression of *AtNDPK2* in *poplar* led to elevated phosphorylation levels and NDPK activity, leading to reduced ROS levels in response to environmental stress [57]. NaCl markedly upregulates MAPK9 gene expression, which is highly expressed in guard cells and positively regulates ROS signaling, and the overexpression of *CaMAPK9* significantly enhances the tolerance to salt stress in *Arabidopsis* [58]. Under salt stress, the increased phosphorylation levels of NDPK1, NDPK2, NDPK3 and

MAPK9 enhanced the ability of *L. barbarum* to respond to oxidative stress and maintain cellular homeostasis (Table S1, Fig. 9). Salt stress led to the accumulation of ABA in the leaves of *L. barbarum* (Fig. 8D), activating the SnRK2 and MAPK pathways. Activated SnRK2 promoted H₂O₂ production through NADPH oxidase. H₂O₂ not only amplifies MAPK signaling but also further activates the MAPK cascade, increasing H₂O₂ accumulation, meanwhile, the MAPK pathway likely regulates the expression of antioxidant enzymes to break down excess H₂O₂, maintaining redox balance. Additionally, PP2C acts as a negative regulator of the MAPK pathway [21]. Our study observed increased SnRK2.3/6 phosphorylation, H₂O₂ levels, and decreased PP2C phosphorylation, potentially linking to above effects (Table S1, Fig. 8J). In summary, Overall, ABA modulates *L. barbarum*'s salt stress response via multiple MAPK pathway levels (Fig. 9).

In addition, we also found that other MAPK family proteins reported in the literature exhibited significant phosphorylation. Yeast MPK1/SLT2 can be phosphorylated and activated, helping cells adapt to changes in osmotic pressure and cell wall stress under salt stress [59], and the alfalfa MMK2 and yeast MPK1/SLT2 kinases perform homologous functions [60]. The reduced phosphorylation level of MMK2, a key kinase in the MAPK cascade, in *L. barbarum* under salt stress suggested that its function in the salt stress response was limited (Table S1). YODA, MAPKKK3 and MAPKKK5 have overlapping functions upstream of the MKK4/MKK5-MPK3/MPK6 module, regulating plant immunity and growth [53, 61]. The stability of SPEECHLESS (SPCH) is controlled by the MAPK cascade, and the YODA-MKK4/5-MPK3/MPK6 pathway negatively regulates stomatal development [62, 63]. This study suggested that increased phosphorylation of YODA activated the MAPK cascade, stabilized SPCH and improved stomatal development in *L. barbarum*, moreover, the phosphorylation of MAPKKK3 and MAPKKK5 may increase immunity and growth, helping *L. barbarum* adapt to salt stress (Table S1). Overall, the salt adaptability and salt tolerance of *L. barbarum* improved (Fig. 9).

This study provides relevant protein phosphorylation data for the salt tolerance research of *L. barbarum*, describing various signaling pathways and phosphorylation events involved in the salt stress response. However, there are still many problems that require to further thought and optimization. The 7-day experiment period was too short to capture long-term effects of salt stress on *L. barbarum* seedlings. Additionally, compared with the latest proteomic detection technology, the current method had limitations in sensitivity and resolution, making it hard to comprehensively present

phosphorylation event correlations. Thus, future research should focus on optimizing in these ways: extend the experimental period, set time gradients, detect phosphorylation changes under salt stress systematically, and create detailed time-series maps to reveal the adaptation process. Furthermore, introducing advanced molecular biology and genetic engineering techniques to verify key phosphorylation factors' regulatory roles, comprehensively analyze the salt stress response mechanism, and provide a solid basis for understanding salt tolerance.

Materials and methods

Plant materials and differential NaCl treatments

The seeds of *L. barbarum* (Ningqi No.1 variety) were provided by the Lycium Engineering Technology Research Center of Ningxia Academy of Agricultural and Forestry Sciences. The seeds were sown in a mixed medium (nutrient soil:perlite:vermiculite=1:1:1), cultivated for 30 days in an artificially controlled greenhouse [The growth conditions were 25°C, 60 ± 10% relative humidity, and a 16 h photoperiod with 550 ($\mu\text{mol}\cdot\text{m}^{-2}\cdot\text{s}^{-1}$) photosynthetic photon flux density], transplanted into a hydroponic growth system containing Hoagland nutrient solution and cultivated until the 12–14-leaf stage. Subsequently, healthy seedlings with uniform and stable growth were selected for four types of NaCl stress treatments (0, 100, 200 and 300 mM NaCl treatments). After 7 days of treatment, the leaves from the same part of the seedlings were sampled and stored at -80°C. Each treatment group contained three biological replicates, with 20 seedlings per replicate.

Protein extraction and sample preparation

The total protein of *L. barbarum* leaves was extracted via the Borax/PVPP/Phenol protocol as previously described [64]. The determination of the protein concentration via a BCA (bicinchoninic acid) Protein Assay Kit (Thermo Fisher Scientific, Waltham, MA, USA), and the proteins were separated on a 12% SDS-PAGE. The proteins from each sample were digested via trypsinization with a filter-assisted proteome preparation kit (Thermo Fisher Scientific, Waltham, MA, USA), and the peptides were desalted with C18 cartridges and redissolved in 40 μL of 0.1% formic acid solution after lyophilization, then, peptide quantification was performed.

TMT labeling and enrichment of phosphorylated peptides

A 100 μg peptide mixture from each sample was labeled with TMT (Thermo Fisher Scientific, Waltham, MA, USA) reagent according to the manufacturer's instructions. The peptide solutions from the 12 samples were subsequently lyophilized under vacuum, and the phosphorylated peptides via a High-Select™ Fe-NTA

Phosphopeptide Enrichment Kit (Thermo Fisher Scientific, Waltham, MA, USA). The phosphopeptides were eluted with elution buffer, concentrated under vacuum, and then dissolved in 20 μL of 0.1% formic acid for liquid chromatograph tandem mass spectrometer (LC-MS/MS) analysis.

LC-MS/MS data acquisition and protein identification and quantitative analysis

The phosphopeptides were separated via an Easy nLC system (Thermo Fisher Scientific, Waltham, MA, USA). Peptides were loaded onto a C18 reversed-phase column (Thermo Scientific Easy Column, 10 cm long, 75 μm inner diameter, 3 μm resin) in buffer A (0.1% formic acid) and isolated with a linear gradient of solvent B (84% acetonitrile and 0.1% formic acid) at a flow rate of 300 $\text{nL}\cdot\text{min}^{-1}$. LC-MS/MS analysis was performed on a Q Exactive HF mass spectrometer (Thermo Scientific), which was operated in positive ion mode. The MS data were analyzed via a data-dependent top10 method to dynamically select the most abundant precursor ions from the survey scan (300–1800 m/z) for high-energy collisional dissociation (HCD) fragmentation. Survey scans were acquired at a resolution of 70,000 at m/z 200, the resolution for HCD spectra was set to 17500 at m/z 200, and the isolation width was 2 m/z . The automatic gain control (AGC) target was set to 3e6, and the maximum IT was 10 ms. The dynamic exclusion duration was 40 s. The normalized collision energy was 30 eV, and the underfill ratio was defined as 0.1%.

Identification and quantitation of phosphorylated proteins

All the raw data were searched via the MASCOT engine (Matrix Science, London, UK; version 2.2) embedded into Proteome Discoverer 2.4. Tandem mass spectra were searched against the *L. barbarum* database (https://ftp.ncbi.nlm.nih.gov/genomes/all/GCF/019/175/385/GCF_019175385.1_ASM1917538v2/) [65]. The parameter settings were as follows: enzyme=trypsin, max missed cleavages=2, fixed modifications=carbamidomethyl (C), TMT 6/10/16 plex (N-term) variable modifications=oxidation (M), phospho (S/T/Y), peptide mass tolerance=20 ppm, fragment mass tolerance=0.1 Da, and threshold of FDR for proteins and peptides fixed at 0.01.

Bioinformatic analysis

The DEPPs were identified on the basis of changes in the abundance of each phosphorylated protein. The DEPPs were screened with the criteria fold change ≥ 1.2 (upregulated proteins) or ≤ 0.83 (downregulated proteins) and p value < 0.05 . Then, complexheatmap R (R Version 3.4) was used to classify both the sample and protein expression dimensions and perform cluster analysis on the

phosphorylated peptides. GO analysis (<https://www.geneontology.org>) of the DEPPs was performed via Blast2GO (<https://www.blast2go.com/b2ghome>), and the KEGG database (<https://www.genome.jp/kegg/>) was used to annotate enriched metabolic pathways with p values < 0.05 . Moreover, enrichment analysis via GO annotation or KEGG pathway annotation was performed on the target protein set. Finally, we determined the interaction relationships between the target proteins on the basis of information from the STRING (<http://string-db.org/>) database, generated an interaction network and analyzed it via CytoScape software (version number: 3.2.1).

PRM analysis

Six phosphorylated proteins were randomly selected for quantified via liquid chromatography parallel reaction monitoring mass spectrometry (LC-PRM/MS) analysis at Shanghai Applied Protein Technology Co., Ltd.. In brief, protein extraction and trypsin digestion were performed according to the TMT analysis protocol. A Peptide Retention Time Calibration Mixture (Thermo) of stable isotope peptides was added to each sample as an internal standard reference. Tryptic peptides were applied to C18 stage tips for desalting before they were subjected to reversed-phase chromatography on an Easy nLC-1200 system (Thermo Scientific). The HPLC-separated samples were analyzed via PRM MS using a Q Exactive HF mass spectrometer (Thermo Scientific). The mass spectrometer was operated in positive ion mode, and the parameters were as follows: A full MS1 scan was acquired with a resolution of 70,000 (at 200 m/z), an ACG target value of 3.0×10^{-6} , and a maximum ion injection time of 200 ms. Full MS scans were followed by 20 PRM scans at 35,000 resolution (at 200 m/z) with AGC 3.0×10^{-6} and a maximum injection time of 200 ms. The targeted peptides were isolated with a 1.5 Th window. Ion activation/dissociation was performed at normalized collision energy of 27 in an HCD cell. MS data were processed using Skyline [66]. PRM-MS experiments were performed with three biological replicates per group.

Enzyme activity assays

The activity of enzymes, including FBPase, FBA, TPI, PGK, PDHA and ACC, were measured following the instructions for the kit from Suzhou Coming Biotechnology Co., Ltd. (Suzhou, China). In brief, approximately 0.1 g of the sample was weighed, and 1 mL of extraction solution was added for homogenization in an ice bath and ultrasonication. After centrifugation, the supernatant and working solution were added to a trace quartz cuvette, the absorbance was measured at room temperature, and the enzyme activity was calculated according to the sample protein.

Substance content assays

The determination of glucose content was performed via the phenol-sulfuric acid method [67], with optimization and adjustment to certain experimental procedures. The determination of glucose content was carried out via the phenyl-sulfuric acid method. 1 g leaves were homogenized in 100 mL distilled water, the mixture was centrifuged at $2000 \times g$ for 5 min, and the absorbance at $\lambda = 525$ nm was measured on a visible spectrophotometer (Genesys 10 VIS; Thermo Electro Corporation, Berlin, Germany). The glucose content was calculated on the basis of absorbance extrapolation, and the glucose content was expressed in $\text{nmol} \cdot \text{g}^{-1}$ FW.

NAD⁺ and NADH contents were determined according to the improved method proposed by Wang et al. [68] with optimization and adjustment to certain experimental procedures. 1 g tissue sample was added to 2 mL of 100 mM HCl or NaOH solution for grinding, incubated in a boiling water bath for 5 min, and centrifuged at $10,000 \times g$ for 10 min at 4°C. The supernatant was used to determine the concentrations of NAD⁺ and NADH. The absorbance at 570 nm was evaluated, with the NAD⁺ and NADH contents expressed in $\text{nmol} \cdot \text{g}^{-1}$ FW.

Grind the *L. barbarum* leaves into a fine powder, then add 90% methanol (chromatographic grade) and extract the mixture at 4°C for 12 h, afterward, centrifuge the mixture at $10,000 \times g$ for 5 min. The sample was washed with methanol solution and formic acid, dried under nitrogen, and reconstituted of 40% methanol solution. The contents of ABA, OPDA, JA, JA-ILE and 2HJA were determined via high-performance liquid chromatography-tandem mass spectrometry (HPLC-MS/MS) with an Agilent 1290 high-performance liquid chromatography system coupled with an AB Sciex QTRAP 6500+ mass spectrometer. Elution from the WAX column was performed with 1.5 mL of 80% methanol containing 5% NH₄OH, and the eluate was collected, dried under nitrogen, reconstituted in 100 μL of 40% methanol solution, and analyzed for SA content via HPLC-MS/MS. The chromatographic and mass spectrometric parameters were as previously described [69], and the results are expressed as $\text{ng} \cdot \text{g}^{-1}$ FW.

We adopted and optimized the method used by Wan et al. (2024) to determine the H₂O₂ content [70]. We weighed 1 g leaves, homogenized in acetone extraction solution, and centrifuged to remove solid residues. The extract was reacted with 10% titanium tetrachloride solution and 200 μL of concentrated ammonia and then centrifuged again. The precipitate was washed three times with acetone, and the precipitate was dissolved in concentrated sulfuric acid. The absorbance was measured at 412 nm, and the results are expressed as $\mu\text{mol} \cdot \text{g}^{-1}$ FW.

Statistical analysis

Three independent biological replicates were used for all the measurements in this study. The data are shown as the means \pm standard errors (SEs). One-way ANOVA was performed via SPSS version 26.0, the data were analyzed via least significant difference (LSD) post hoc multiple tests, and $p < 0.05$ was considered to indicate statistical significance.

Conclusions

This study conducted comprehensive physiological and phosphorylation proteomic analysis on *L. barbarum* leaves under different concentrations of NaCl stress. We found that *L. barbarum* responded to salt stress by regulating glycolysis, plant hormone signal transduction, and MAPK signal transduction. Salt stress activated the glycolysis pathway of *L. barbarum* by regulating the activity of related enzymes through protein phosphorylation, promoting glucose metabolism to obtain energy. The accumulation of ABA, JA, and SA contents induced by salt stress triggered protein phosphorylation events in the plant hormone signaling pathway, and the activation and regulation of MAPK signaling pathway mediated by phosphorylated proteins initiated downstream salt stress response factors. This study provided adaptation and coping strategies for *L. barbarum* in saline environments, which was essential for developing salt-resistant genetic resources.

Supplementary Information

The online version contains supplementary material available at <https://doi.org/10.1186/s12870-025-06402-3>.

Supplementary Material 1.
Supplementary Material 2.
Supplementary Material 3.
Supplementary Material 4.

Acknowledgements

The authors would like to show great appreciation to Applied Protein Technology Co., LTD (Shanghai, China) for the phosphoproteomic analysis in this study.

Authors' contributions

W.L. and Z.Z. were the primary authors of the manuscript, they acquired, organized the data, and performed the initial data interpretation. W.Y. performed the experiments. Q.Z., N.Y., S.Y. and J.Z. were major contributor for analyzing data and text check. B.W. was contributor to drawing and continually modifying Figs and contributed analysis tools. L.W. and W.L. were contributors to article modification and experimental design, W.L. and is the main corresponding author. All authors have read and approved the manuscript.

Funding

This work was supported by the National Natural Science Foundation of China (Award No. 32301632), Natural Science Foundation of Ningxia Hui Autonomous Region (Award No. 2024AAC03097; 2023AAC05024) and Graduate Innovation Project of Ningxia University (Award No. CXXM202458).

Data availability

The mass spectrometry proteomics data have been incorporated into the iProX Integrated Proteome Resources, the proteomeXchange ID is PXD058720.

Declarations

Ethics approval and consent to participate

The experimental research on plants performed in this study complies with institutional, national and international guidelines.

Consent for publication

Not applicable.

Competing interests

The authors declare no competing interests.

Received: 10 December 2024 Accepted: 13 March 2025

Published online: 31 March 2025

References

- Hao SH, Wang YR, Yan YX, Liu YH, Wang JY, Chen S. A review on plant responses to salt stress and their mechanisms of salt resistance. *Horticulturæ*. 2021;7(6):132.
- Li ZH, Zhong F, Guo JR, Chen Z, Song J, Zhang Y. Improving wheat salt tolerance for saline agriculture. *J Agric Food Chem*. 2022;70(48):14989–5006.
- An YX, Wang ZQ, Liu BJ, Cao YW, Chen L. Translational landscape of *Medicago truncatula* seedlings under salt stress. *J Agric Food Chem*. 2023;71(44):16657–68.
- Rajappa S, Krishnamurthy P, Huang H, Yu DJ, Friml Jí, Xu J, Kumar PP. The translocation of a chloride channel from the Golgi to the plasma membrane helps plants adapt to salt stress. *Nat Commun*. 2024;15(1):3978.
- Gong ZZ, Xiong LM, Shi HZ, Yang SH, Herrera-Estrella LR, Xu GH, Chao DY, Li JR, Wang PY, Qin F, et al. Plant abiotic stress response and nutrient use efficiency. *Sci China Life Sci*. 2020;63(5):635–74.
- Zhang H, Zhao Y, Zhu JK. Thriving under stress: how plants balance growth and the stress response. *Dev Cell*. 2020;55(5):529–43.
- Jia C, Huang YK, Cheng ZC, Zhang N, Shi TZ, Ma X, Zhang GR, Zhang C, Hua RM. Combined transcriptomics and metabolomics analysis reveals profenofos-induced invisible injury in pakchoi (*Brassica rapa* L.) through inhibition of carotenoid accumulation. *Agric Food Chem*. 2024;72(27):15321–33.
- Yu ZP, Duan XB, Luo L, Dai SJ, Ding ZJ, Xia GM. How plant hormones mediate salt stress responses. *Trends Plant Sci*. 2020;25(11):1117–30.
- Zhang WJ, Zhou YW, Zhang Y, Su YH, Xu TD. Protein phosphorylation: a molecular switch in plant signaling. *Cell Rep*. 2023;42(7): 112729.
- Liu C, Jiang X, Yuan Z. Plant responses and adaptations to salt stress: a review. *Horticulturæ*. 2024;10(11):1221.
- Suzuki M, Hashioka A, Mimura T, Ashihara H. Salt stress and glycolytic regulation in suspension-cultured cells of the mangrove tree, *Bruguiera sexangula*. *Physiol Plant*. 2005;123(3):246–53.
- Pan JW, Li Z, Wang QG, Guan YA, Li XB, Huangfu YG, Meng FH, Li JL, Dai SJ, Liu W. Phosphoproteomic profiling reveals early salt-responsive mechanisms in two foxtail millet cultivars. *Front Plant Sci*. 2021;12: 712257.
- Yang YQ, Guo Y. Unraveling salt stress signaling in plants. *J Integr Plant Biol*. 2018;60(9):796–804.
- Zhang YJ, Dong WK, Ma HL, Zhao CX, Ma FQ, Wang Y, Zheng XL, Jin MH. Comparative transcriptome and coexpression network analysis revealed the regulatory mechanism of *Astragalus cicer* L. in response to salt stress. *BMC Plant Biol*. 2024;24(1):817.
- Wang P, Li ZW, Wei JS, Zhao ZL, Sun DY, Cui SJ. A Na⁺/Ca²⁺ exchanger-like protein (AtNCL) involved in salt stress in *Arabidopsis*. *J Biol Chem*. 2012;287(28):44062–70.
- Bakshi A, Choi WG, Kim SH, Gilroy S. The vacuolar Ca²⁺ transporter CATION EXCHANGER 2 regulates cytosolic calcium homeostasis, hypoxic signaling, and response to flooding in *Arabidopsis thaliana*. *New Phytol*. 2023;240(5):1830–47.

17. Chen J, Wang LH, Yuan M. Update on the roles of rice MAPK cascades. *Int J Mol Sci.* 2021;22(4):1679.
18. Takahashi F, Mizoguchi T, Yoshida R, Ichimura K, Shinozaki K. Calmodulin-dependent activation of MAP kinase for ROS homeostasis in *Arabidopsis*. *Mol Cell.* 2011;41(6):649–60.
19. Wurzing B, Mair A, Pfister B, Teige M. Cross-talk of calcium-dependent protein kinase and MAP kinase signaling. *Plant Signal Behav.* 2011;6(1):8–12.
20. Su SQ, Jiang YM, Zhu X, Yu SB, Wang FX, Xue L, Cui HT. Calcium-dependent protein kinase 5 and 13 enhance salt tolerance in rice by directly activating OsMPK3/6 kinases. *Plant Physiol.* 2024;196(4):3033–47.
21. Danquah A, Zelicourt AD, Colcombet J, Hirt H, BE Frebort I, Dolezel J. The role of ABA and MAPK signaling pathways in plant abiotic stress responses. *Biotechnol Adv.* 2014;32(1):40–52.
22. Drerup MM, Schlucking K, Hashimoto K, Manishankar P, Steinhörst L, Kuchitsu K, Kudla J. The calcineurin b-like calcium sensors CBL1 and CBL9 together with their interacting protein kinase CIPK26 regulate the *Arabidopsis* NADPH oxidase RBOHF. *Mol Plant.* 2013;6(2):559–69.
23. Lin Z, Li Y, Wang YB, Liu XL, Ma L, Zhang ZJ, Mu C, Zhang Y, Peng L, Xie SJ, et al. Initiation and amplification of SnRK2 activation in abscisic acid signaling. *Nat Commun.* 2021;12(1):2456.
24. Liu Y, Yu TF, Li YT, Zheng L, Lu ZW, Zhou YB, Chen J, Chen M, Zhang JP, Sun GZ, et al. Mitogen-activated protein kinase TaMPK3 suppresses ABA response by destabilising TaPYL4 receptor in wheat. *New Phytol.* 2022;236(1):114–31.
25. Tian YL, Xia T, Qiang X, Zhao YX, Li SP, Wang YM, Zheng Y, Yu JW, Wang JX, Wang M. Nutrition, bioactive components, and hepatoprotective activity of fruit vinegar produced from Ningxia wolfberry. *Molecules.* 2022;27(14):4422.
26. Liu XX, Zheng R, Radani Y, Gao H, Yue SJ, Fan WQ, Tang JN, Shi J, Zhu JZ. Transcriptional deciphering of the metabolic pathways associated with the bioactive ingredients of wolfberry species with different quality characteristics. *BMC Genomics.* 2023;24(1):658.
27. Liu X, Gao H, Radani Y, Yue SJ, Zhang ZP, Tang JN, Zhu JZ, Zheng R. Integrative transcriptome and metabolome analysis reveals the discrepancy in the accumulation of active ingredients between *Lycium barbarum* cultivars. *Planta.* 2024;259(4):74.
28. Xu X, Zheng GQ, Zhou T, Hui HX. Research on character of physiology and biochemistry and salt-tolerance of wolfberry in ochr-sierozems soil of Ningxia. *Chinese J Eco-Agric.* 2002;10(03):74–7.
29. Yao XC, Meng LF, Zhao WL, Mao GL. Changes in the morphology traits, anatomical structure of the leaves and transcriptome in *Lycium barbarum* L. under salt stress. *Front Plant Sci.* 2023;14:1090366.
30. Yuan H, Liu K, Wang CM, Xie HC, Li HJ, Jia H. The differences between two cultivars of *Lycium barbarum* in osmotic stress tolerance and salt tolerance. *Pratacultural Sci.* 2016;33(4):681–90.
31. Zhang ZZ, He KN, Zhang T, Tang D, Li RJ, Jia SF. Physiological responses of goji berry (*Lycium barbarum* L.) to saline-alkaline soil from Qinghai region, china. *Sci rep.* 2019;9(1):12057.
32. Li WN, Rao SP, Du C, Liu LP, Dai GL, Chen JH. Strategies used by two goji species, *Lycium ruthenicum* and *Lycium barbarum*, to defend against salt stress. *Sci Hortic.* 2022;306:111430.
33. Wen J, Xu K, Ji DH, Xu Y, Chen CS, Wang WL, Xie CT. The mechanism of maintaining intracellular homeostasis in the red alga *Pyropia haitanensis* under hyposaline stress. *Front Mar Sc.* 2022;9: 928617.
34. Nariya H, Inouye S. Activation of 6-phosphofructokinase via phosphorylation by Pkn4, a protein ser/thr kinase of *Myxococcus xanthus*. *Mol Microbiol.* 2002;46(5):1353–66.
35. Wang WL, Zheng HY, Wen J, Xu K, Xu Y, Ji DH, Chen CS, Xie CT. Early signaling events in the heat stress response of *Pyropia haitanensis* revealed by phosphoproteomic and lipidomic analyses. *Algal Res.* 2022;67: 102837.
36. Muñoz EB, Luna-Vital DA, Fornasini M, Baldeón ME, Mejía EGD. Gamma-conglutin peptides from andean lupin legume (*Lupinus mutabilis* Sweet) enhanced glucose uptake and reduced gluconeogenesis in vitro. *J Funct Foods.* 2018;45:339–47.
37. Kim SC, Guo L, Wang XM. Nuclear moonlighting of cytosolic glyceraldehyde-3-phosphate dehydrogenase regulates *Arabidopsis* response to heat stress. *Nat Commun.* 2020;11(1):3439.
38. Liu YD, Chen J, Lin DB. Phosphoproteomic analysis highlights phosphorylation of primary metabolism-related proteins in response to postharvest cold storage and subsequent shelf-life in tomato fruit. *Postharvest Biol Tec.* 2023;205: 112486.
39. Massange-Sanchez JA, Casados-Vazquez LE, Juárez-Colunga S, Sawers R, Tiessen A. The phosphoglycerate kinase (PGK) gene family of maize (*Zea mays* var. B73). *Plants-Basel.* 2020;9(12):1639.
40. Kolitsida P, Nolic V, Zhou J, Stumpe M, Niemi NM, Dengjel J, Abeliovich H. The pyruvate dehydrogenase complex regulates mitophagic trafficking and protein phosphorylation. *Life Sci Alliance.* 2023;6(9): e202302149.
41. Hasan H, Abd Rahim MH, Campbell L, Carter D, Abbas A, Montoya A. Overexpression of acetyl-CoA carboxylase in *Aspergillus terreus* to increase lovastatin production. *New Biotech.* 2018;44:64–71.
42. Edel KH, Kudla J. Integration of calcium and ABA signaling. *Curr Opin Plant Biol.* 2016;33:83–91.
43. Mittler R, Blumwald E. The roles of ROS and ABA in systemic acquired acclimation. *Plant Cell.* 2015;27(1):64–70.
44. Kim TW, Youn JH, Park TK, Kim EJ, Park CH, Wang ZY, Kim SK, Kim TW. OST1 activation by the brassinosteroid-regulated kinase CDG1-LIKE1 in stomatal closure. *Plant Cell.* 2018;30(8):1848–63.
45. Yuan F, Yang HM, Xue Y, Kong DD, Ye R, Li CJ, Zhang JY, Theprung-sirikul L, Shrift T, Krichilsky B, et al. OSCA1 mediates osmotic-stress-evoked Ca²⁺ increases vital for osmosensing in *Arabidopsis*. *Nature.* 2014;514(7522):367–71.
46. Wang PC, Zhao Y, Li ZP, Hsu CC, Liu X, Fu LW, Hou YJ, Du YY, Xie SJ, Zhang CG, et al. Reciprocal regulation of the TOR kinase and ABA receptor balances plant growth and stress response. *Mol Cell.* 2018;69(1):100–12.
47. Mouna G, Al BF, Anket S, Marco L. Role of jasmonic acid in plants: the molecular point of view. *Plant Cell Rep.* 2021;40(8):1471–94.
48. Hazman M, Hause B, Eiche E, Nick P, Riemann M. Increased tolerance to salt stress in OPDA-deficient rice ALLENE OXIDE CYCLASE mutants is linked to an increased ROS-scavenging activity. *J Exp Bot.* 2015;66(11):3339–52.
49. Liu YY, Du MM, Deng L, Shen JF, Fang MM, Chen Q, Lu YH, Wang QM, Li CY, Zhai QZ. MYC2 regulates the termination of jasmonate signaling via an autoregulatory negative feedback loop. *Plant Cell.* 2019;31(1):106–27.
50. Zhu J, Wang WS, Yan DW, Hong LW, Li TT, Gao X, Yang YH, Ren F, Lu YT, Yuan TT. CK2 promotes jasmonic acid signaling response by phosphorylating MYC2 in *Arabidopsis*. *Nucleic Acids Res.* 2023;51(2):619–30.
51. Salem MA, Giavalisco P. Mutation in the *Arabidopsis* regulatory-associated protein TOR1B (RAPTOR1B) leads to decreased jasmonates levels in leaf tissue. *Plant Signal Behav.* 2019;14(10): e1649567.
52. Lu CF, Liu XY, Tang YQ, Fu YQ, Zhang JM, Yang LT, Li PH, Zhu ZL, Dong P. A comprehensive review of TGA transcription factors in plant growth, stress responses, and beyond. *Int J Biol Macromol.* 2024;258: 128880.
53. Siddhi KJ, Alok KS. ROS mediated MAPK signaling in abiotic and biotic stress-striking similarities and differences. *Front Plant Sci.* 2015;6:769.
54. Long HJ, Li ZY, Suo H, Ou LJ, Miao W, Deng WQ. Study on the mechanism of grafting to improve the tolerance of pepper to low temperature. *Agronomy.* 2023;13(5):1347.
55. Zhang TG, Li QL, Diao ZH, Li P, Wang J, Zheng S. Effects of salt and drought stresses on antioxidant system and *RbohC* and *RbohF* genes expression in *Brassica campestris*. *J Appl Ecol.* 2019;30(3):969–78.
56. Asai S, Ohta K, Yoshioka H. MAPK signaling regulates nitric oxide and NADPH oxidase-dependent oxidative bursts in *Nicotiana benthamiana*. *Plant Cell.* 2008;20(5):1390–406.
57. Zhang JX, Movahedi A, Sang M, Wei ZH, Xu JJ, Wang XL, Wu XL, Wang MY, Yin TM, Qiang ZG. Functional analyses of NDKP2 in *Populus trichocarpa* and overexpression of *PtNDPK2* enhances growth and tolerance to abiotic stresses in transgenic poplar. *Plant Physiol Bioch.* 2017;117:61–74.
58. Jammes F, Song C, Shin DJ, Munemasa S, Takeda K, Gu D, Cho D, Lee S, Giordo R, Sritubtim S, et al. MAP kinases MPK9 and MPK12 are preferentially expressed in guard cells and positively regulate ROS-mediated ABA signaling. *PNAS.* 2009;106(48):20520–5.
59. Yurko N, Liu X, Yamazaki T, Hoque M, Tian B, Manley JL. MPK1/SLT2 links multiple stress responses with gene expression in budding Yeast by phosphorylating Tyr1 of the RNAP II CTD. *Mol Cell.* 2017;68(5):913–25.
60. Jonak C, Kiegerl S, Lloyd C, Chan J, Hirt H. MMK2, a novel alfalfa MAP kinase, specifically complements the Yeast MPK1 function. *Mol Gen Genet.* 1995;248(6):686–94.
61. Wang YP, Wu YY, Zhang HL, Wang PX, Xia YJ. *Arabidopsis* MAPKK kinases YODA, MAPKKK3, and MAPKKK5 are functionally redundant in development and immunity. *Plant Physiol.* 2022;190(1):206–10.

62. Sun TJ, Nitta Y, Zhang Q, Wu D, Tian HN, Lee JS, Zhang YL. Antagonistic interactions between two MAP kinase cascades in plant development and immune signaling. *Embo Rep.* 2018;19(7): e45324.
63. Putarjunan A, Ruble J, Srivastava A, Zhao CZ, Rychel AL, Hofstetter AK, Tang XB, Zhu JK, Tama F, Zheng N, et al. Bipartite anchoring of SCREAM enforces stomatal initiation by coupling MAP kinases to SPEECHLESS. *Nat Plants.* 2019;5(7):742–54.
64. Wang XC, Li XF, Deng X, Han HP, Shi WL, Li YX. A protein extraction method compatible with proteomic analysis for the eukaryote *Salicornia europaea*. *Electrophoresis.* 2007;28(21):3976–87.
65. Cao YL, Li YL, Fan YF, Li Z, Yoshida K, Wang JY, Ma XK, Wang N, Mitsuda N, Kotake T, et al. Wolfberry genomes and the evolution of Lycium (Solanaceae). *Commun Biol.* 2021;4(1):671.
66. MacLean B, Tomazela DM, Shulman N, Chambers M, Finney GL, Frewen B, Kern R, Tabb DL, Liebner DC, MacCoss MJ. Skyline: an open source document editor for creating and analyzing targeted proteomics experiments. *Bioinformatics.* 2010;26(7):966–8.
67. Chow PS, Landhausser SM. A method for routine measurements of total sugar and starch content in woody plant tissues. *Tree Physiol.* 2004;24(10):1129–36.
68. Wang D, Ma Q, Li WY, Aalim H, Luo ZS. Moderation of respiratory cascades and energy metabolism of fresh-cut pear fruit in response to high CO₂ controlled atmosphere. *Postharvest Biol Tec.* 2021;172: 111379.
69. Matsuura H, Aoi A, Satou C, Nakaya M, Masuta C, Nabeta K. MS analysis of endogenous jasmonic acid, salicylic acid, and their related compounds. *Plant Growth Regul.* 2009;57(3):293–301.
70. Wan JH, Wu YT, Tong ZT, Su WB, Lin HT, Fan ZQ. Melatonin treatment alleviates chilling injury of loquat fruit via modulating ROS metabolism. *Foods.* 2024;13(19):3050.

Publisher's Note

Springer Nature remains neutral with regard to jurisdictional claims in published maps and institutional affiliations.